Toward Functional Type III [Fe]-Hydrogenase Biomimics for H_2 Activation: Insights from Computation

Kevin A. Murray,[a] Dr. Matthew D. Wodrich,[a] Prof. Dr. Xile Hu,[b]* Prof. Dr. Clémence Corminboeuf[a]*

[a]Laboratory for Computational Molecular Design and [b]Laboratory of Inorganic Synthesis and Catalysis, Institut des Sciences et Ingénierie Chimiques, Ecole Polytechnique Fédérale de Lausanne, CH-1015 Lausanne, Switzerland

Address correspondence to: clemence.corminboeuf@epfl.ch (CC), xile.hu@epfl.ch (XH)

ABSTRACT

The chemistry of [Fe]-hydrogenase has attracted significant interest due to its ability to activate molecular hydrogen. The intriguing properties of this enzyme have prompted synthesis of numerous small molecule mimics aimed at activating H_2. Despite considerable effort, a majority of these compounds remain nonfunctional for hydrogenation reactions. Using a recently synthesized model as an entry point, seven biomimetic complexes were examined via DFT computations to probe the influence of ligand environment on the ability of a mimic to bind and split H_2. One mimic, featuring a bidentate diphosphine group incorporating an internal nitrogen base, was found to have particularly attractive energetics, prompting study of the role played by the proton/hydride acceptor necessary to complete the catalytic cycle. Computations revealed an experimentally accessible energetic pathway utilizing a benzaldehyde proton/hydride acceptor along with the most promising catalyst.

INTRODUCTION

The chemistry underlying enzymes that activate molecular hydrogen have received considerable interest,[1] as their small biomimetic model counterparts represent a potential clean hydrogen source.[2] Type III [Fe]-hydrogenases, formally named H_2-forming methylenetetrahydromethopterin dehydrogenase (Hmd), catalyze the reversible reduction of methyenyltetrahydromethanopterin (MPT^+) with H_2 to methylenetetrahydromethanopterin (HMPT) and H^+ (Figure 1). During this cycle, a hydride ion, produced via heterolytic H_2 splitting, is stereospecifically transferred to the *pro*-R face of MPT^+ to form HMPT.[3] This process is an intermediary step in the reduction of CO_2 to methane by methanogens grown under nickel-limiting conditions.[4]

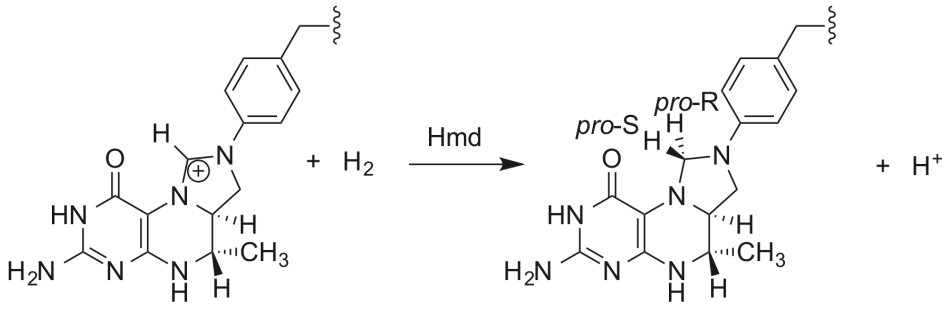

Figure 1. Reaction of methyenyltetrahydromethanopterin (MPT^+) and H_2 to methylenetetrahydromethanopterin (HMPT) and H^+ catalyzed by Hmd. The stereospecific addition of the hydride ion occurs to the *pro*-R face.

Crystallographic and spectroscopic studies have determined the [Fe]-Hydrogenase active site to be either five- (square pyramidal) or six-coordinate (octahedral): the central iron atom is coordinated to a cysteine sulfur atom, two *cis*-CO ligands, a bidentate pyridine cofactor, and a solvent molecule (Figure 2).[3, 5] Notwithstanding some uncertainty, the current consensus tends toward an active enzyme that is a five-coordinate square pyramid.[5g, 5i] The prospective uses for the product of [Fe]-Hydrogenase motivated the production of numerous small molecule mimics.[6],[7] While earlier mimics were six-coordinate in nature, Hu and coworkers[6q] recently provided a *five-coordinate*, square-pyramidal Fe^{II} model complex that closely resembles the enzyme active site (Figure 2). Unfortunately, these mimics, in general, are incapable of binding molecular hydrogen.

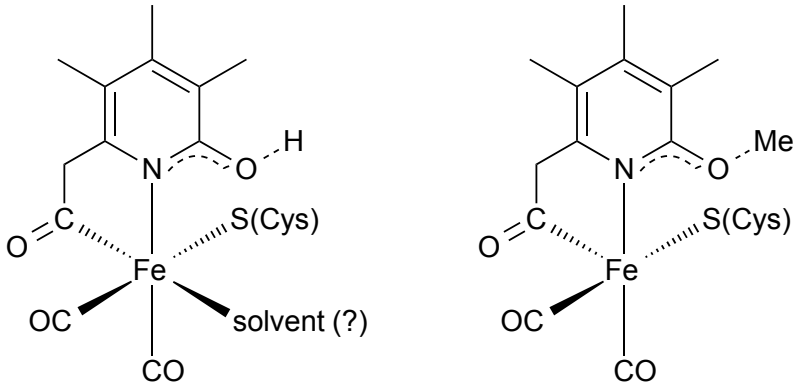

Figure 2. Proposed active site of [Fe]-Hydrogenase and a prototypical model complex.

Computation has also played a role in understanding both structure and function of [Fe]- and [FeFe]-hydrogenases and related mimetic compounds. For instance, Nakatani and co-workers used density functional computations to predict several possible active site structures for [Fe]-hydrogenase based on the assignment of CO stretching frequencies.[8] CO and CN frequencies were once again employed by Dey,[9] Reiher,[10] as well as Darensbourg and Hall,[11] to elucidate additional structural details of both mono- and dimetallic hydrogenases. Theoretically determined ^{57}Fe Mössbauer spectroscopy has contributed toward the same objective.[12] Hu[13] recently probed small molecule/ligand binding using a biomimetic [Fe]-hydrogenase to better understand the effects played by the stereoelectronic environment surrounding the central iron atom.

Likewise, detailed mechanistic information regarding the catalytic cycles of mono- and dimetallic hydrogenases has been unraveled using density functional computations.[9, 14] Based on an early crystal structure that was subsequently refined to show that only a single, not two, empty coordination sites were present in the Hmd active site,[5f] Yang and Hall[14a] (YH) first proposed a "trigger" mechanism to explain the cleavage of H_2 in the presence of MPT^+. To account for the significant change in the active site structure, YH revised their mechanism in 2009,[14b] where the MPT^+ substrate no longer directly interacts with the Fe center. Instead, MPT^+ effectively caps the active site, enclosing the H_2 molecule and, after heterolytic cleavage, acts as a hydride acceptor. YH concluded that the role of the Fe-complex was to capture H_2 and form the hydride ion, while MPT^+ functions as a hydride acceptor. The purpose of this contribution is to provide a detailed analysis of the energetics surrounding the binding and heterolytic splitting of H_2 as well as the subsequent removal of the hydride ion and proton by several different [Fe]-hydrogenase biomimetic systems related to that synthesized by Hu et al.[6q] We stress that our goal is not to predict faithful structural models of [Fe]-hydrogenase, which are limited in flexibility, but rather to determine how systematically replacing biological ligands by synthetic counterparts can

result in models capable of activating H_2 in the absence of the biological environment. By proceeding in this manner, our hope is to predict attractive synthetic targets possessing desired properties that may ultimately lead to biomimetic compounds capable of H_2 activation.

COMPUTATIONAL METHODS

Molecular geometries were optimized at the M06/def2-SVP level[15] and invoked Cramer and Truhlar's SMD[16] polarizable continuum model[17] for tetrahydrofuran (THF, ε=7.4257) in Gaussian09.[18] Frequency calculations on optimized geometries provided unscaled free energy corrections, as well as insured structures were minima (zero imaginary frequencies) or transition states (one imaginary frequency) on the potential energy surface. To obtain refined energy estimates and assess the important role of long-range dispersion interactions, single point energies were computed using the B3LYP[19] density functional appended with a density-dependent dispersion correction, B3LYP-dDsC.[20] B3LYP-dDsC computations used a Slater type orbital triple-ζ basis set, TZ2P, in ADF.[21],[22] Note that the dDsC scheme has been successfully applied to diverse chemical problems.[23] In particular, the density dependence of both the dispersion coefficient and the damping function is valuable for describing charged species[24] and transition metals.[25] The accuracy of the B3LYP-dDsC computations has been confirmed through examination of M06/TZ2P free energies (see supporting information). All reported free energies include electronic energies obtained from computations at the B3LYP-dDsC/TZ2P//M06/def2-SVP, B3LYP/TZ2P//M06/def2-SVP (see supporting information), or M06/TZ2P//M06/def2-SVP (see supporting information) level, free energy corrections at the M06/def2-SVP level, and solvation corrections using Klamt's continuum model for realistic solvents (COSMO-RS[26]). M06/def2-SVP geometric, vibrational, and energy computations used the "Ultrafine" grid to remove known problems with the size of the integration grid.[27] The dissection of energies into

donor/acceptor roles between the Fe center and H_2 were determined using block-localized wavefunction-energy decomposition analysis (BLW-EDA[28]), also known as absolutely-localized molecular orbitals-charge transfer analysis (ALMO-CTA[29]) at the M06/def2-SVP level in Q-Chem.[30]

A relevant question is how use of an *a posteriori* dispersion correction affects the free energies of H_2 binding and activation, as well as other steps in the catalytic cycle. To address this issue, free energies were also determined using the standard B3LYP functional, in addition to B3LYP-dDsC. Not surprisingly, large differences in the reaction free energies are observed between the standard and dispersion corrected B3LYP variants, particularly for the steps of the catalytic process involving association of two molecules/ions. Describing these weakly associated complexes requires an accurate description of non-bonded interactions, which can be accomplished using dispersion corrected functional. Computations using the M06 functional, which partially accounts for these weak dispersion interactions via its design and parameterization, show similar trends to the dispersion corrected B3LYP (B3LYP-dDsC) values, thereby validating our use of a dispersion corrected density functional.

RESULTS AND DISCUSSION

Seven [Fe]-Hydrogenase biomimetic compounds were selected for detailed analysis based on different criteria: mimic **a**[6q] has previously been synthesized by Hu and coworkers, while others (**b**-**g**) were chosen to probe the influences accompanying modification of the stereoelectronic environment surrounding the iron center (mimics **b**-**f**) as well as alteration of the internal base (mimic **g**), Figure 3. In summary, mimic **a** possesses a bidentate pyridine ligand mimicking the enzyme cofactor, two *cis*-CO ligands, and a S-Aryl moiety representing the cysteine sulfur atom. Due to its close structural similarity to the enzyme active site, this structure is referred to as the "wild-type" (WT) mimic. In mimic **b** (also referred to as 3CO), the S-Aryl ligand in mimic **a** has been substituted by a third CO ligand. Based on their modified π-accepting ability, phosphine ligands were selectively substituted for various ligands of

the WT structures to create mimics **c**-**e**. In **c** (PMe) the WT S-Aryl moiety has been substituted with a PMe_3 ligand, while for mimics **d** and **e**, the S-aryl moiety and the CO ligand *trans* to the pyridine cofactor nitrogen have each been replaced with two PMe_3 ligands (**d**, 2PMe) or a bidentate ligand in which two phosphine groups are linked by an ethyl spacer, $–P(Me)_2CH_2CH_2(Me)_2P-$ (**e**, 2PEt). Finally, mimic **f** (SPMe) retains the S-Aryl moiety of the WT mimic and substitutes a PMe_3 for a CO ligand trans to the thiolate, while mimic **g** (2PN) represents a modified version of mimic **e** in which a NH group has been incorporated into the C-C bond of the bidentate ligand, $–P(Me)_2CH_2NHCH_2(Me)_2P-$. Aside from allowing additional conformational flexibility, this nitrogen can also act as an internal base, facilitating the heterolytic splitting of H_2 in a manner similar to the sulfur atom in the WT mimic.

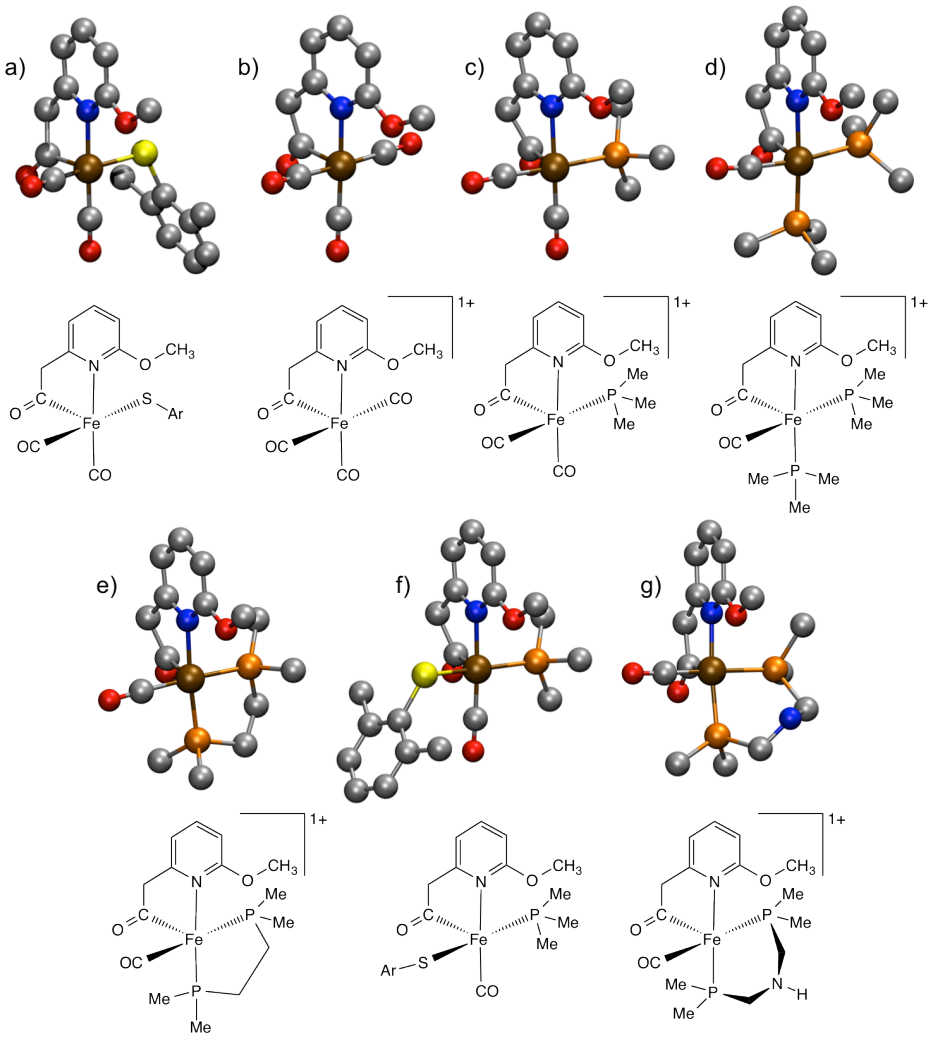

Figure 3. Computed 3D structures of the [Fe]-H mimics studied (hydrogen atoms omitted). Wild-type (**a**), 3CO (**b**), PMe (**c**), 2PMe (**d**), 2PEt (**e**), SPMe (**f**), 2PN (**g**). Atom color code: silver=carbon, red=oxygen, blue=nitrogen, yellow=sulfur, orange=phosphorus, brown=iron.

H_2 Binding. The binding of H_2 to the biomimetic complexes is the first critical step toward completing the Hmd catalyzed reaction depicted in Figure 1. Naturally, one key requirement for this reaction to proceed is an exergonic or mildly endergonic reaction free energy that governs the association of H_2 to the biomimetic Fe complex (Figure 4, **1→2**). Table 1 shows the binding free energies of H_2 to each of the biomimetic complexes (**a**-**g**). The results can be delineated between those compounds possessing a thiolate ligand (**a**, **f**) and those mimics in which this ligand has been replaced by an alternative. Both mimics **a** and **f** are characterized by very unfavorable H_2 binding free energies (10.2 and 8.3 kcal/mol, respectively), that are the highest among the seven mimics tested and are in agreement with previous computational results on the enzyme active site.[9] On the other hand, those mimics lacking a thiolate moiety each show H_2 binding free energies of less than 6 kcal/mol. This represents a significant improvement toward experimental accessibility that likely arises due to the cationic nature of the complex that permits the iron center to become more electrophilic. Mimic **b**, which contains three strongly π-accepting CO ligands has an H_2 binding value of 3.2 kcal/mol. While this weakly endergonic value is already promising, modifications of the ligands surrounding the iron center likely will subtly influence the stereoelectonics of a particular mimic potentially leading to more favorable H_2 binding energies. Following this strategy, the CO ligands of mimic **b** were successively replaced with weaker π-accepting phosphine groups, which should facilitate charge transfer stabilization of the H_2/Mimic due to the increased electron density on the iron center. This hypothesis is confirmed by examination of the Hirshfeld charges, which show increasing electron density on the iron atom along the series: 3CO (**b**) < PMe (**c**) < 2PMe (**d**) < 2PEt (**e**) < 2PN (**g**) (see SI for values). While substituting one or two CO ligand by an equivalent number of PMe_3 groups slightly raises the H_2 binding free energy (5.1 kcal/mol, mimic **c** and 3.6 kcal/mol, mimic **d**), the amount of charge transfer between the mimic and H_2 does increase, as

indicated by ALMO-CTA computations (Table 2). Mimics **e** and **g** each contain a bidentate ligand incorporating two phosphine groups linked by an ethyl group (**e**) or a -CH_2-NH-CH_2- moiety (**g**). These compounds further benefit from increased charge transfer (Table 2). The binding free energies of both these species are quite remarkable, having values of 1.4 and 1.7 kcal/mol, respectively, which is five times lower than the WT mimic (**a**).

Table 1. Free energy values computed at the B3LYP-dDsC/TZ2P//M06/def2-SVP level in implicit THF solvent (COSMO-RS) for the catalytic cycle leading to the splitting/formation of H_2 by the proposed biomimics. Values in kcal/mol.

Mimic	**H_2 binding**	**Imidazole Association**	**H_2 splitting**	
	1→2	**2→2'**	**2→TS2,3**	**TS2,3→□**
WT (**a**)	10.17	--	15.68	-3.84
3CO (**b**)	3.16	3.31	1.90	-15.11
Pmethyl (**c**)	5.10	5.01	-0.33	-6.23
2Pmethyl (**d**)	3.64	6.12	3.29	-1.98
2Pethyl (**e**)	1.44	4.09	4.14	-0.34
SPmethyl (**f**)	8.31	--	23.62	-9.21
2PN (**g**)	1.68	--	3.54	-1.94

Table 2. Charge transfer analysis (ALMO-CTA) of H_2 binding with the seven biomimetic models. Computations at the M06/def2-SVP level, gas phase binding electronic energies computed at the B3LYP-dDsC/TZ2P//M06/def2-SVP level. Value in kcal/mol.

	Charge Transfer	**Binding Electronic Energy**
WT Mimic (**a**)	-23.00	1.44
3CO Mimic (**b**)	-25.67	-8.76
PMe Mimic (**c**)	-26.59	-8.83
2PMe Mimic (**d**)	-27.39	-11.38
2PEt Mimic (**e**)	-28.83	-12.27
2SPMe Mimic (**f**)	-27.39	0.96
2PN Mimic (**g**)	-30.21	-11.66

Imidazole Association. For mimics lacking an internal base, it is necessary to associate an additional ion/molecule that permits the heterolytic cleavage of H_2 to proceed by acting as a proton acceptor. For

our purposes 1-methylimidazole was chosen to serve as a prototypical proton acceptor. This choice seems appropriate, given the nearly equivalent reaction free energy of the biological system (Figure 5). For mimics **b**, **c**, **d**, and **e**, it is necessary to form a complex between the mimic and the imidazole (**2→2',** Figure 4) before H_2 splitting can occur. Accomplishing this results in a significant entropy penalty, which causes the corresponding reaction free energies for the overall association process to be endergonic for each of the four mimics (Table 1). The free energies of this process range from 3.3 to 6.1 kcal/mol, thereby creating a problematic step in advancing the catalytic process beyond this point.

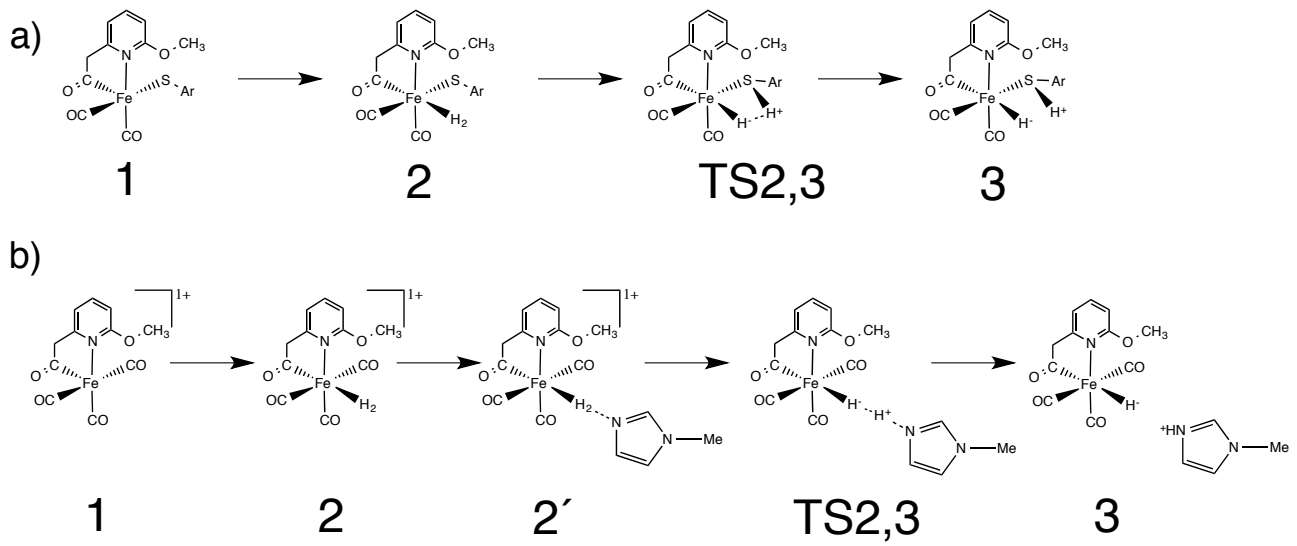

Figure 4. Reaction pathways for the binding and heterolytic splitting of H_2. For those mimics containing an internal base (pathway a, WT mimic depicted) the process proceeds via direct binding (**1→2**) and internal splitting (**2→TS2,3**). For mimics lacking an internal base (pathway b, 3CO mimic depicted) an extra step is required (**2→2'**) which involves association of the proton accepting 1-methylimidazole molecule.

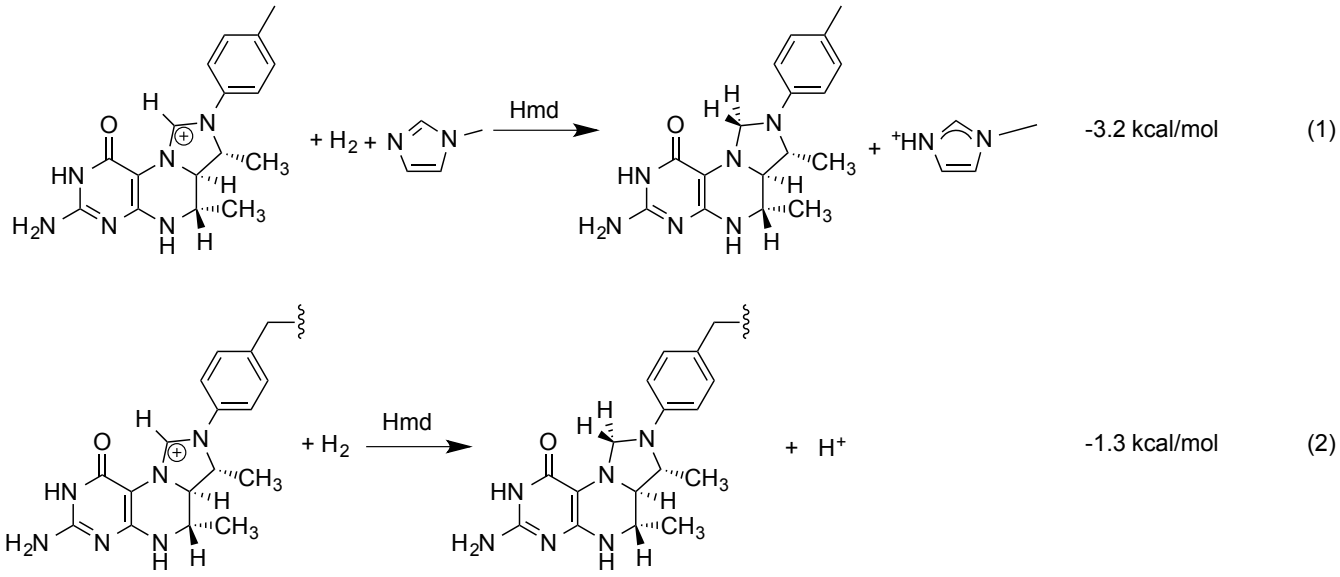

Figure 5. The reaction free energy HMD-catalyzed H_2 splitting with MPT^+ and 1-methylimidizole as the proton acceptor (**1**) and the biological system (**2**).

Heterolytic H_2 Splitting. After H_2 binding and imidazole association (if necessary, vide supra) to the biomimetic complexes, the next step in completing the Hmd catalyzed reaction is heterolytic cleavage of H_2 (Figure 4, **2→TS2,3**).[9, 14b] Ideally, this process should be associated with a low energy transition state (TS) barrier and a sufficiently exergonic overall reaction free energy that prevents reformation of H_2. For the splitting step, each of the mimics (**a**-**g**) are separated into two categories, those containing and those lacking an internal base. Compounds **a**, **f**, and **g** each possess an internal base that can act as a proton acceptor during H_2 cleavage (Figure 4a). Since compounds **b**, **c**, **d**, and **e** lack this internal feature, H_2 is split using the mimic/imidazole complex (Figure 4b). Table 1 shows the free energies associated with heterolytic H_2 cleavage for each biomimetic complex (**a**-**g**). The WT mimic (**a**), is characterized by an endergonic energy of 15.7 kcal/mol for the $\mathbf{2_a}$**→TS2,3**$_\mathbf{a}$ splitting reaction and a mildly exergonic **TS2,3**$_\mathbf{a}$**→3**$_\mathbf{a}$ step (3.8 kcal/mol). In contrast, for the 3CO mimic (**b**) the energy required for H_2 splitting is relatively modest (1.9 kcal/mol, $\mathbf{2_b}$**→TS2,3**$_\mathbf{b}$) and is accompanied by significant stabilization of the product, **3** (-15.1 kcal/mol). As with H_2 binding, the modified stereoelectronics accompanying replacement of CO by PMe_3 ligands also alters the ability of a mimic to split H_2.

Substituting one CO ligand of the 3CO (mimic **b**) to a PMe_3 group (mimic **c**) results in a negligible TS barrier (**2_c→TS2,3_c**, -0.3 kcal/mol[31]) and a stabilization of the products by ~6 kcal/mol (**TS2,3_c→3_c**). Mimics with two phosphine groups (**d** and **e**) slightly increase the TS barrier relative to the single phosphine mimic (**c**), yielding values of 3.3 kcal/mol and 4.1 kcal/mol, respectively. However, the products for both **d** and **e** are relatively unstable (Table1) and would likely quickly reform the reactant species.

For those mimics possessing internal bases, replacing one WT CO ligands with a PMe_3 ligand (mimic **f**) results in a dramatic increase in the required H_2 splitting energy (**2_f→TS2,3_f**, 23.6 kcal/mol). The highly endergonic splitting value sharply contrasts the behavior of 2PN mimic (**g**), which maintains an impressively low TS barrier of only 3.5 kcal/mol (**2_g→TS2,3_g**). Importantly, a TS barrier of this height can easily be overcome in an experimental environment. While the **TS2,3_g→3_g** step is only exergonic by 1.9 kcal/mol, the exceptionally low overall **1→3** reaction free energy clearly identifies this mimics as the most promising of the seven tested (Figure 6). This is particularly true given that it is not necessary to form a 3-component reaction complex (mimic + H_2 + imidazole, as required for mimics **b**-**e**) to heterolytically split H_2. Given that the ultimate objective of this study is identification of an energetically feasible full catalytic cycle leading to H_2 production, further discussion is restricted to mimics **a** and **g**. The latter owing to its exceptionally small H_2 binding and splitting free energies and the former to serve as reference to assess the magnitude of improvements made upon the original model.

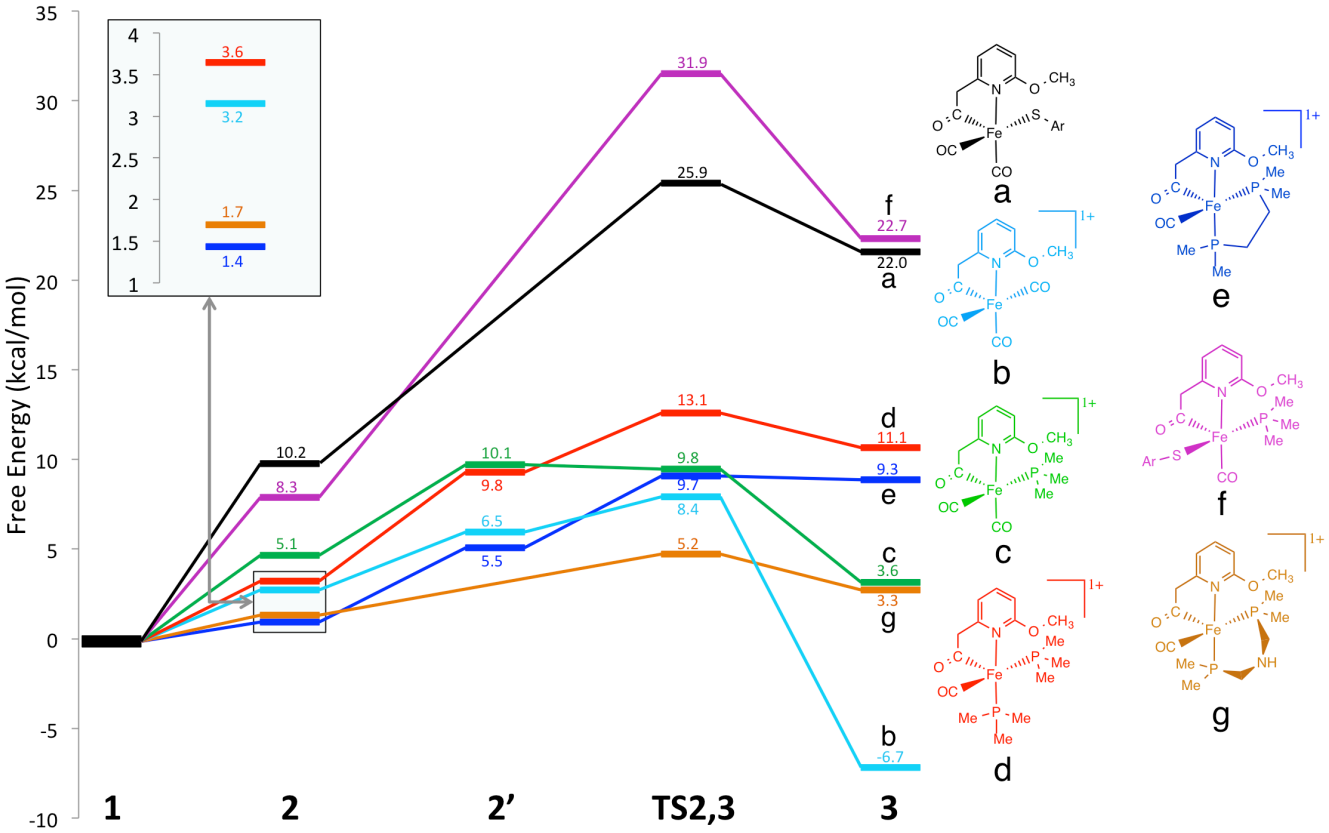

Figure 6. Reaction free energy profiles [B3LYP-dDsC/TZ2P//M06/def2-SVP level in implicit THF solvent (COSMO-RS)] for hydrogen binding (**1→2**), 1-methylimidazole association (**2→2'**), heterolytic H_2 cleavage (**2→TS2,3→3** or **2'→TS2,3→3**) for the seven biomimics. Values in kcal/mol.

Catalytic Cycle with a Truncated MPT⁺ Model. The Hmd catalyzed reaction pathways determined for the biomimetic compounds examined here are roughly based upon the proposal of Yang and Hall.[14b] Figures 7a and 7b illustrate the potential pathways for the WT (**a**) and 2PN mimics (**g**), including the binding/splitting of H_2 and subsequent hydride/proton transfer from the mimic to a truncated MPT⁺ substrate (Figure 8a) and 1-methylimidazole (Figure 8b), respectively. The catalytic cycle begins either through direct coordination of H_2 into the empty coordination site of the 5-coordinate biomimic (**1**), forming a η^2-H_2 Fe-complex (**2**) or by binding of the MPT⁺ substrate (**10**) followed by H_2 insertion (**7**). After binding (**1→2**), H_2 is heterolytically cleaved via one of two pathways. The first pathway (**2→TS2,3→3**) discussed earlier, involves only H_2 and the biomimetic complex, which is succeeded by association of the MPT⁺ substrate (**3→4**). The second pathway (**7→TS7,4→4**) involves the assistance of

the MPT^+ substrate in H_2 cleavage. For this alternative pathway to be viable the dissociation constant for the bound MPT^+/mimic complex (**1→10** or **2→7**) must be slow to allow sufficient time for H_2 activation to occur (**7→TS7,4→4**). Both the first and second pathways recombine at **4**, where heterolytic H_2 cleavage has formed a hydride ion bonded to the Fe-center and a proton bonded to the acceptor base (S-Aryl, mimic **a**). From structure **4**, the hydride and proton generated from the heterolytic splitting of H_2 must be transferred from the complex to the corresponding hydride/proton acceptors in one of two ways. The first (**4→TS4,5→5**, Figure 7a**)** involves an initial hydride transfer to the accepting MPT^+ ion (**5)** followed by proton transfer to a 1-methylimidazole (**5→6**) or by dissociation of the MPT^+ substrate (**5→9**). In the later case, the proton remains bound to the base and is then abstracted from **9** by 1-methylimidizole, closing the catalytic cycle. The second distinct pathway (**4→8→TS8,6→6**, Figure 7a) involves proton (**8**) followed by hydride transfer (**6**). From **6**, the catalyst/HMPT complex dissociates, reforming **1**.

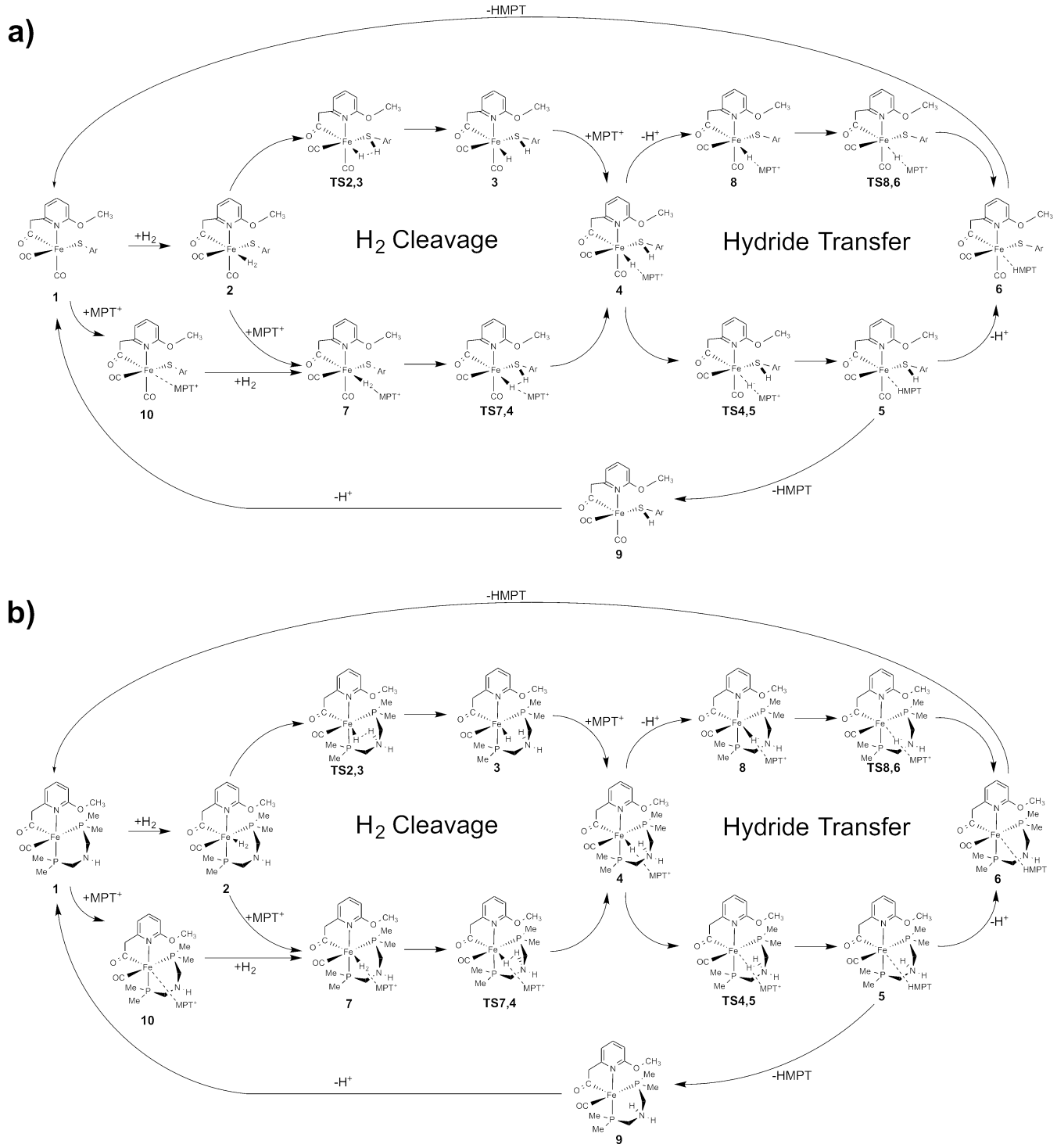

Figure 7. Possible reaction pathways for the heterolytic cleavage of H_2 by the wild-type (a) and 2PN biomimics (b) using a truncated MPT^+ substrate as a hydride acceptor and 1-methylimidazole as a proton acceptor.

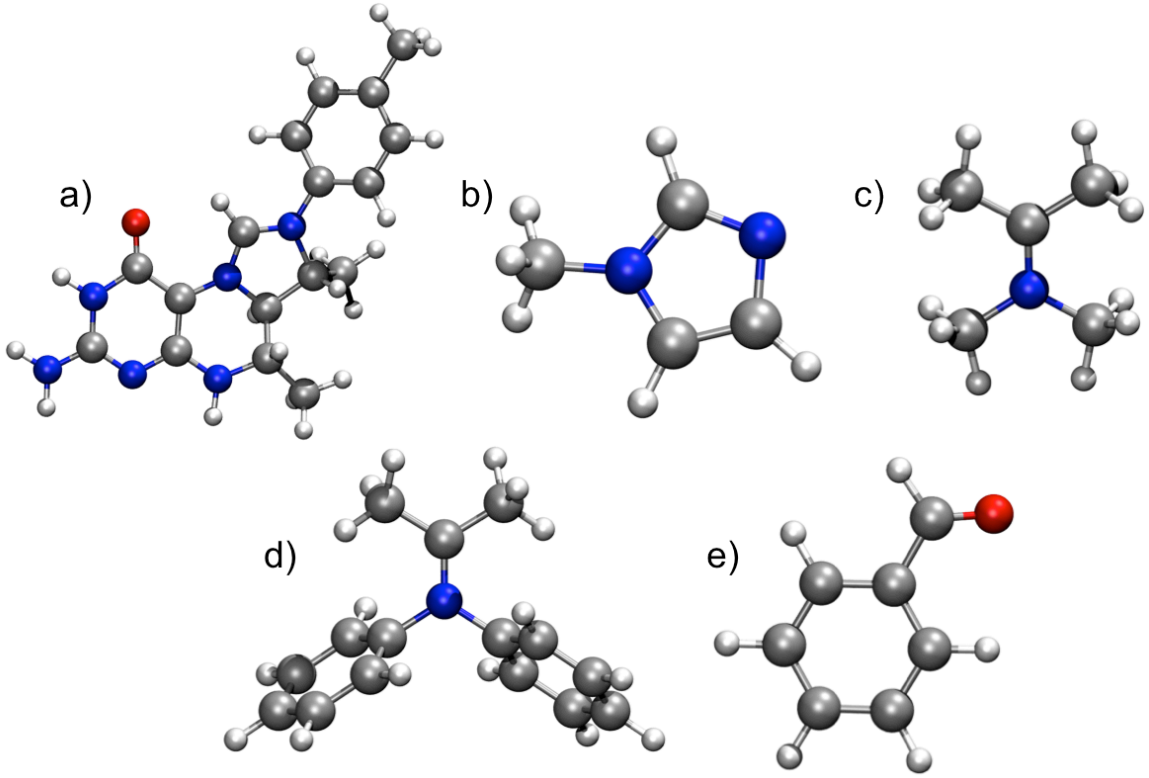

Figure 8. 3-D representation of the hydride/proton acceptors used in this study: (**a**) MPT^+ mimic, (**b**) 1-methylimidizole, (**c**) methyliminium, (**d**) phenyliminium, (**e**) benzaldehyde.

The reaction free energy profiles for the catalytic cycle of the WT and the 2PN mimics are shown in Figures 9 and 10. For the WT mimic (Figure 9) the energetically preferred pathway involves direct H_2 association to the 5-coordinate iron compound (**1→2**) followed by heterolytic cleavage (**2→TS2,3→3**) and MPT^+ association (**3→4**). The route that includes addition of MPT^+ followed by H_2 association and cleavage pathway (**1→10→7→4**) is less favorable. The hydride transfer process occurs spontaneously from the iron center to MPT^+ upon deprotonation of the sulfur-aryl moiety by 1-methylimidazole (**4→6**). Dissociation of HMPT then reforms **1** in an exergonic process. For the WT mimic, intermediate **8** is not a stable point on the potential energy surface. Overall, the highest energy point on the profile is **4**, which requires 26.3 kcal/mol of energy. It is this overall endergonicity, in addition to the unfavorable free energies of H_2 binding and splitting steps, that explains and rationalizes the non-functionality of the WT mimic, as experimentally demonstrated by Hu and co-workers.[6q] In

contrast, the 2PN mimic (Figure 10) presents a markedly improved energetic profile for H_2 binding and splitting (**1→2→3**, vide supra). The association of MPT^+ (**3→4**) remains exothermic. From **4** the most favorable pathway for reformation of the catalyst involves nitrogen deprotonation by 1-methylimidazole (**8**) followed by hydride transfer from the iron to MPT^+ (**8→TS8,6→6**), which represents the highest point on the most energetically favorable pathway. HMPT dissociation then reforms **1**. While the energetics of this cycle are still not ideal, they do represent an improvement of over 5 kcal/mol in comparison to the WT mimic (**a**).

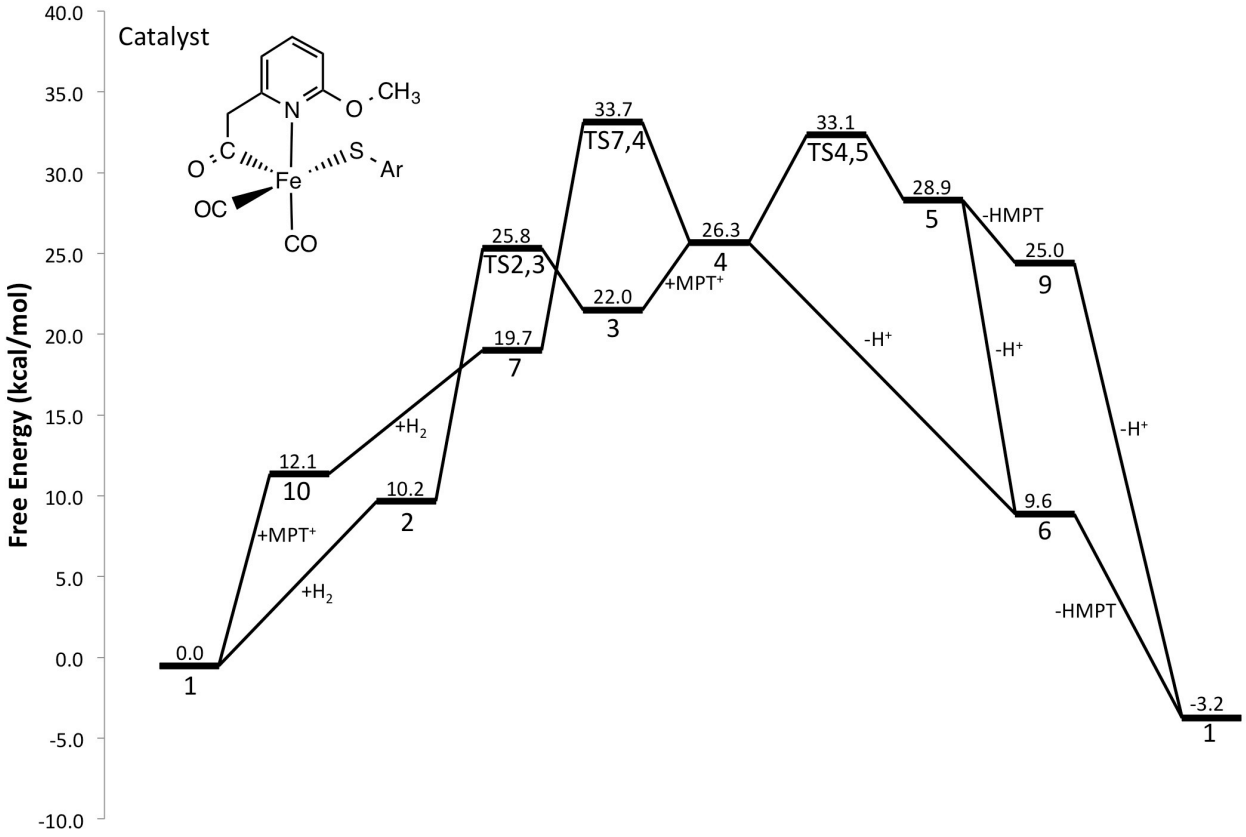

Figure 9. Reaction free energy profiles [computed at the B3LYP-dDsC/TZ2P//M06/def2-SVP level in implicit THF solvent (COSMO-RS)] for the catalytic cycle of the WT mimic (**a**) using a truncated MPT^+ model and 1-methylimidazole as the hydride and proton receptors, respectively. Values in kcal/mol. Compound numbers correspond to structures presented in Figure 7a.

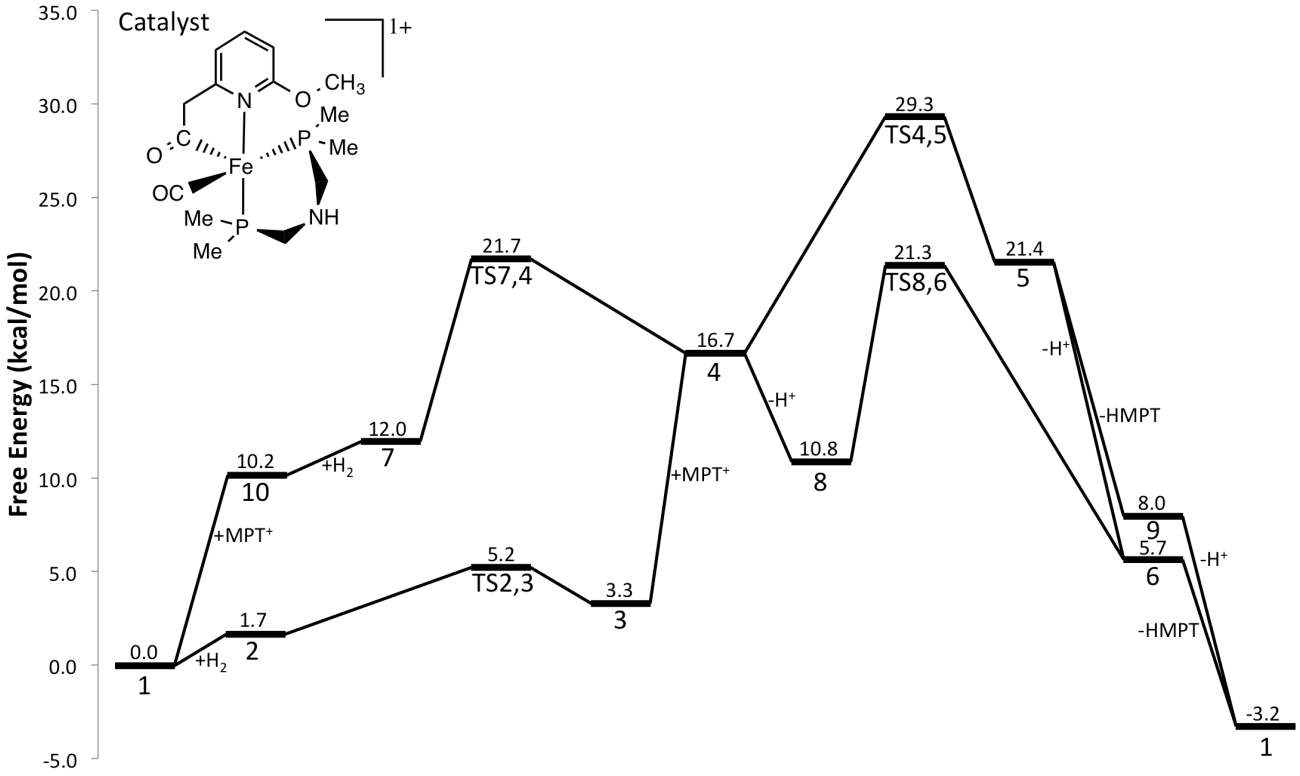

Figure 10. Reaction free energy profiles [computed at the B3LYP-dDsC/TZ2P//M06/def2-SVP level in implicit THF solvent (COSMO-RS)] for the catalytic cycle of the 2PN mimic (**g**) using a truncated MPT^+ model and 1-methylimidazole as the hydride and proton receptors, respectively. Values in kcal/mol. Compound numbers correspond to structures presented in Figure 7b.

Catalytic Cycle with Small Molecule/Ion Substrates. As illustrated by Figure 10, the 2PN mimic (**g**) possesses a more appealing energetic profile relative to its wild-type counterpart. Conceivably, one way to further tune the reaction pathway energetics is not by alteration of the catalyst itself, but by replacing the large MPT^+ substrate with different molecules or ions that could serve as improved hydride/proton acceptors. This option is particularly appealing due to the potential of having a single substrate that could act as both a proton and hydride acceptor, in contrast to the two species [MPT^+ (hydride acceptor) and imidazole (proton acceptor)] employed earlier. Following this approach, three replacements for the MPT^+ substrate have been examined with 2PN mimic. The three substrates represent both positively charged (methyl- and phenyliminium, Figures 8c and d) and neutral species (benzaldehyde, Figure 8e). The corresponding reaction free energy profiles involving the most favorable energetic pathways are

presented in Figure 11 and summarized in Table 3. Both the red and blue pathways in Figure 11 correspond to replacement of the MPT^+ substrate with a positively charged iminium compound. Naturally, each of these profiles maintains the favorable initial steps involving H_2 binding and splitting that are associated with only the 2PN mimic itself (black pathway, Figure 11). The binding energies of the iminium complexes with the mimic shows that reducing steric bulk decreases the binding free energy, as illustrated by the methyliminium compound with a value of 7.5 kcal/mol (**3→4** blue pathway in Figure 11 and Table 3) versus the bulkier phenyliminium with a value of 16 kcal/mol. Once the acceptor substrate has formed a complex with the catalyst, removal of the hydride ion by the either iminium acceptor is quite unfavorable (**4→TS4,5**, Table 3), despite the electrophilic nature of the iminium ion. This large energy barrier likely arises more from the prominent geometric displacement required to adopt the TS geometry from **4** (see Cartesian Coordinates in the SI) and less from the actual accepting ability of iminium ion. Subsequent proton removal, also by the iminium compound, first involves a reorientation of the iminium acceptor (**5→5´**) flowed by overcoming an energetically negligible TS barrier (Table 3 and Figure 11). Overall, the height of the TS barriers associated with hydride removal makes the use of the iminium compounds as proton/hydride acceptors energetically no better than the original MPT^+ substrate.

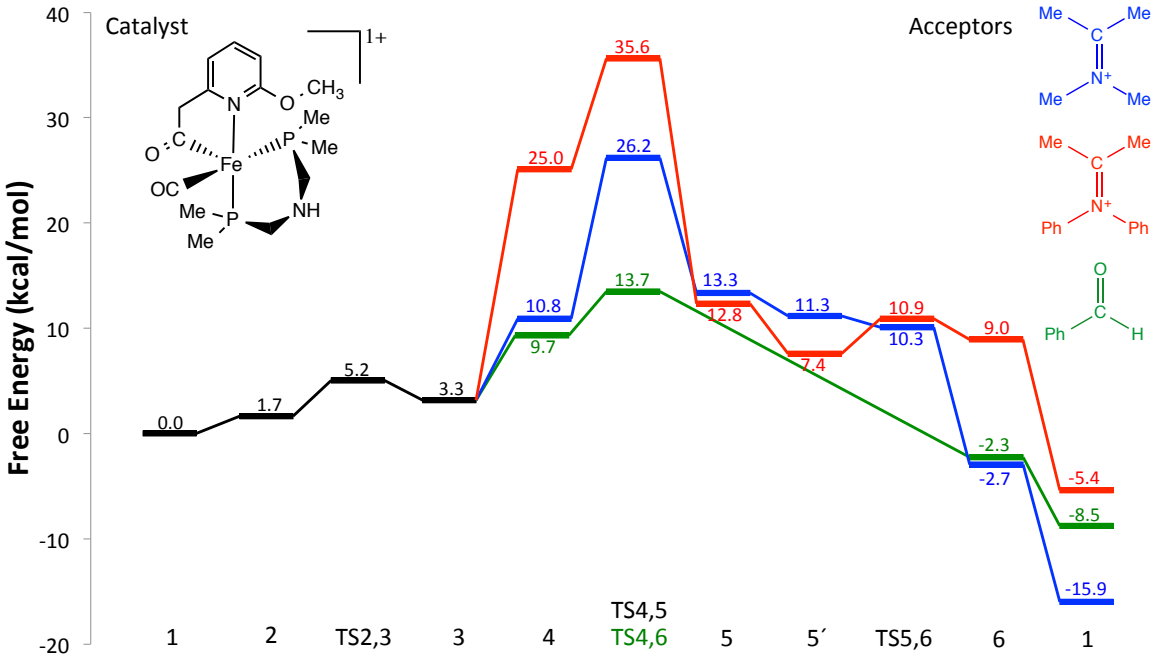

Figure 11. Reaction free energy profiles at the B3LYP-dDsC/TZ2P//M06/def2-SVP level in implicit THF solvent (COSMO-RS) for the methyliminium (blue), phenyliminium (red), and benzaldehyde (green) hydride/proton acceptors with the 2PN mimic. The hydrogen capture and splitting steps, which are common for each of the substrates, are represented in black.

Table 3. Free energy values at the B3LYP-dDsC/TZ2P//M06/def2-SVP level in implicit THF solvent (COSMO-RS) for relevant reactions during the catalytic cycle for various proton/hydride acceptor substrates with the 2PN mimic (**g**). Values in kcal/mol.

Ligand	methyliminium	phenyliminium	benzaldehyde
3 → 4	7.5	21.7	6.5
4 → TS4,5	15.4	10.6	--
TS4,5 → 5	-12.9	-22.8	--
5 → 5´	-2.0	-5.4	
5´ → TS5,6	-1.0[a]	3.5	--
TS5,6 → 6	-13.1	-1.9	--
4 → TS4,6	--	--	3.9
TS4,6 → 6	--	--	-15.9
6 → 1	-13.2	-14.4	-13.7

a) +0.2 kcal/mol at the M06/def2-SVP level

A second option is to utilize a neutral molecule, rather than a cationic acceptor substrate. Indeed, the catalyst/acceptor substrate binding free energy is only 6.4 kcal/mol for benzaldehyde (green pathway, Figure 11). Rather than undergoing a stepwise process to remove the hydride ion and proton, benzaldehyde accepts both entities in a concerted process (**4→TS4,6**, Figure 11), thereby coverting the aldehyde to an alcohol through a mechanism similar to the coversion of ketones to alcohols by Milstein's iron pincer complexes.[32] Incredibly, removal of the hydride ion/proton is associated with a very small TS barrier of less than 4 kcal/mol (Figure 11 and Table 3). The newly formed alcohol complex then easily dissociates (**6→1**), reforming the original catalyst in an energetically favorable process. For the 2PN mimic using the aldehyde acceptor substrate, the entire process of H_2 binding, splitting, and removal of the product ions can be accomplished with less than 14 kcal/mol of energy, as illustrate in Figure 11 (green pathway) and Figure 12. The outstanding energetics of the 2PN mimic (**g**) renders this mimic/acceptor substrate combination an energetically superior alternative to previously synthesized systems.

One further way to tuning catalytic cycle energetics available to experimentalists is through variation of the solvent. While the discussions above have been restricted to THF (the solvent used in the experimental work that prompted this study), the influence that changing the solvent to either methanol or dichloromethane was also examined for potential energetic improvements. Table 4 provides free energies of each reaction step along the catalytic cycle for the 2PN (**g**) mimic with a benzaldehyde acceptor. The use of THF or methanol as a solvent lead to value that are roughly equivalent, although THF appears slightly preferable to methanol based on a slightly depressed 4→TS4,6 free energy. Regardless, the differences between these two solvents appear to be energetically trivial. This contrasts the free energies when dichloromethane is employed, which yield significantly increased barrier height for the 2→TS2,3 and, to a lesser degree, the 4→TS4,6 steps. Thus, our computations indicate that using

THF as a solvent leads to the lowest free energy pathway over the catalytic cycle of the three solvents tested.

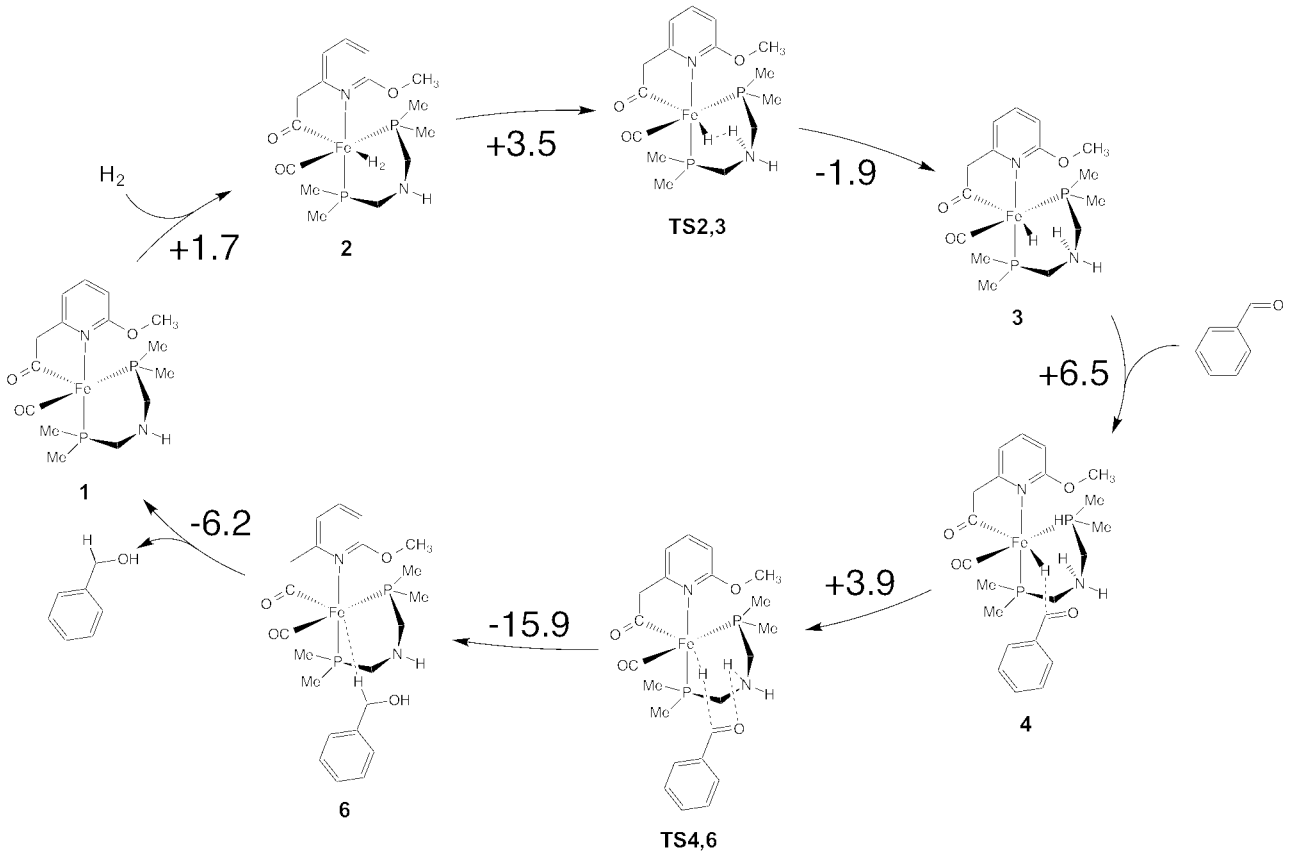

Figure 12. Overview of the catalytic cycle involving the 2PN biomimic (**g**) with an aldehyde acceptor substrate. Free energies computed at the B3LYP-dDsC/TZ2P//M06/def2-SVP level in implicit THF solvent (COSMO-RS). Values in kcal/mol.

Table 4. Influence of solvent on the various reaction steps in the catalytic cycle using the 2PN mimic as the catalyst and benzaldehyde as a proton/hydride acceptor. Free energies computed at the B3LYP-dDsC/TZ2P//M06/def2-SVP level in implicit THF, methanol, or dichloromethane solvent (COSMO-RS). Values in kcal/mol.

Reaction	**THF**	**Methanol**	**Dichloromethane**
1 → 2	1.68	1.59	1.77
2 → TS2,3	3.53	3.52	8.53
TS2,3 → 3	-1.93	-1.85	1.56
3 → 4	6.45	6.37	4.60
4 → TS4,6	3.93	4.41	5.26
TS4,6 → 6	-15.91	-15.66	-21.98
6 → 1	-6.20	-6.18	-5.37

CONCLUSIONS

The energetics surrounding the binding and heterolytic splitting of H_2 by a series of seven [Fe]-hydrogenase biomimetic compounds has been examined. Modification of the iron center stereoelectronic environment through substitution of selected ligands alters the ability of a biomimic to bind molecular hydrogen. In particular, replacing highly π-accepting CO ligands by weaker π-accepting phosphine ligands yielded more favorable H_2 binding energies. Examination of the energetics associated with each of the seven biomimetic compounds identified one mimic containing a bidentate phosphine ligand with an internal nitrogen base (mimic **g**) as having an enhanced energetic profile. Based upon this finding, the subsequent steps involving removal of the proton and hydride ions to reform the catalyst were determined. While the hydride/proton acceptor combination of a truncated MPT^+ with 1-methylimidazole, as well iminium compounds capable of accepting both a hydride ion and proton were found be energetically unfavorable, a neutral benzaldehyde that accepts the hydride ion/proton in a concerted process possesses an experimentally accessible energetic profile. Based on this analysis, the combination of the [Fe]-hydrogenase mimic featuring a bidentate phosphine ligand with an internal nitrogen base and an aldehyde proton/hydride acceptor represents an appealing new starting point toward the synthesis of functional biomimetics capable of H_2 activation and hydrogenation.

ACKNOWLEDGMENTS

KAM gratefully acknowledges the Paul B. and Mildred Seydel Foundation as well as the Fulbright US Student Program for financial support. XH acknowledges the Swiss National Science Foundation

(SNSF) for financial support (Grant 200020_152850/1). CC acknowledges the EPFL and SNSF (Grant 20021_137529) for financial support.

Supporting Information. 3-dimensional structures of selected compounds, reaction free energy profiles of the WT mimic with methyliminium, phenyliminium, and benzaldehyde are provided. Electronic energies, free energies corrections, solvation energies, and Cartesian coordinates (in .xyz format) of all compounds are also provided.

REFERENCES

[1] W. Lubitz, H. Ogata, O. Rüdiger and E. Reijerse, *Chem. Rev.* **2014**, *114*, 4081-4148.
[2] a) F. A. Armstrong and J. C. Fontecilla-Camps, *Science* **2008**, *321*, 498-499; b) G. J. Kubas, *Chem. Rev.* **2007**, *107*, 4152-4205; c) P. M. Vignais and B. Billoud, *Chem. Rev.* **2007**, *107*, 4206-4272; d) J. C. Fontecilla-Camps, A. Volbeda, C. Cavazza and Y. Nicolet, *Chem. Rev.* **2007**, *107*, 4273-4303; e) A. L. De Lacey, V. M. Fenandez, M. Rousset and R. Cammack, *Chem. Rev.* **2007**, *107*, 4304-4330; f) K. A. Vincent, A. Parkin and F. A. Armstrong, *Chem. Rev.* **2007**, *107*, 4366-4413; g) P. E. M. Siegbahn, J. W. Tye and M. B. Hall, *Chem. Rev.* **2007**, *107*, 4414-4435.
[3] a) E. J. Lyon, S. Shima, R. Boecher, R. K. Thauer, F. W. Grevels, E. Bill, W. Roseboom and S. P. J. Albracht, *J. Am. Chem. Soc.* **2004**, *126*, 14239-14248; b) S. Shima, E. J. Lyon, M. S. Sordel-Klippert, M. Kauss, J. Kahnt, R. K. Thauer, K. Steinbach, X. L. Xie, L. Verdier and C. Griesinger, *Angew. Chem. Int. Ed.* **2004**, *43*, 2547-2551.
[4] R. K. Thauer, A. R. Klein and G. C. Hartmann, *Chem. Rev.* **1996**, *96*, 3031-3042.
[5] a) S. Shima, E. J. Lyon, R. K. Thauer, B. Mienert and E. Bill, *J. Am. Chem. Soc.* **2005**, *127*, 10430-10435; b) M. Korbas, S. Vogt, W. Meyer-Klaucke, E. Bill, E. J. Lyon, R. K. Thauer and S. Shima, *J. Biol. Chem.* **2006**, *281*, 30804-30813; c) O. Pilak, B. Mamat, S. Vogt, C. H. Hagemeier, R. K. Thauer, S. Shima, C. Vonrhein, E. Warkentin and U. Ermler, *J. Mol. Biol.* **2006**, *358*, 798-809; d) Y. S. Guo, H. X. Wang, Y. M. Xiao, S. Vogt, R. K. Thauer, S. Shima, P. I. Volkers, T. B. Rauchfuss, V. Pelmenschikov, D. A. Case, E. E. Alp, W. Sturhahn, Y. Yoda and S. P. Cramer, *Inorg. Chem.* **2008**, *47*, 3969-3977; e) S. Shima, O. Pilak, S. Vogt, M. Schick, M. S. Stagni, W. Meyer-Klaucke, E. Warkentin, R. K. Thauer and U. Ermler, *Science* **2008**, *321*, 572-575; f) T. Hiromoto, K. Ataka, O. Pilak, S. Vogt, M. S. Stagni, W. Meyer-Klaucke, E. Warkentin, R. K. Thauer, S. Shima and U. Ermler, *FEBS Lett.* **2009**, *583*, 585-590; g) T. Hiromoto, E. Warkentin, J. Moll, U. Ermler and S. Shima, *Angew. Chem. Int. Ed.* **2009**, *48*, 6457-6460; h) M. Salomone-Stagni, F. Stellato, C. M. Whaley, S. Vogt, S. Morante, S. Shima, T. B. Rauchfuss and W. Meyer-Klaucke, *Dalton Trans.* **2010**, *39*, 3057-3064; i) S. Shima, S. Vogt, A. Gobels and E. Bill, *Angew. Chem. Int. Ed.* **2010**, *49*, 9917-9921.
[6] a) J. A. Wright, P. J. Turrell and C. J. Pickett, *Organometallics* **2010**, *29*, 6146-6156; b) X. F. Wang, Z. M. Li, X. R. Zeng, Q. Y. Luo, D. J. Evans, C. J. Pickett and X. M. Liu, *Chem. Commun.* **2008**, 3555-

3557; c) P. J. Turrell, J. A. Wright, J. N. T. Peck, V. S. Oganesyan and C. J. Pickett, *Angew. Chem. Int. Ed.* **2010**, *49*, 7508-7511; d) B. Li, T. Liu, C. V. Popescu, A. Bilko and M. Y. Darensbourg, *Inorg. Chem.* **2009**, *48*, 11283-11289; e) A. M. Royer, T. B. Rauchfuss and D. L. Gray, *Organometallics* **2009**, *28*, 3618-3620; f) A. M. Royer, M. Salomone-Stagni, T. B. Rauchfuss and W. Meyer-Klaucke, *J. Am. Chem. Soc.* **2010**, *132*, 16997-17003; g) S. Tanino, Y. Ohki and K. Tatsumi, *Chem. Asian J.* **2010**, *5*, 1962-1964; h) T. B. Liu, B. Li, C. V. Popescu, A. BIlko, L. M. Perez, M. B. Hall and M. Y. Darensbourg, *Chem. Eur. J.* **2010**, *16*, 3083-3089; i) B. V. Obrist, D. F. Chen, A. Ahrens, V. Schunemann, R. Scopelliti and X. L. Hu, *Inorg. Chem.* **2009**, *48*, 3514-3516; j) D. F. Chen, R. Scopelliti and X. L. Hu, *J. Am. Chem. Soc.* **2010**, *132*, 928-929; k) D. F. Chen, R. Scopelliti and X. L. Hu, *Angew. Chem. Int. Ed.* **2010**, *49*, 7512-7515; l) D. F. Chen, A. Ahrens-Botzong, V. Schunemann, R. Scopelliti and X. L. Hu, *Inorg. Chem.* **2011**, *50*, 5249; m) D. F. Chen, R. Scopelliti and X. L. Hu, *Angew. Chem. Int. Ed.* **2012**, *51*, 1919-1921; n) B. Hu, D. F. Chen and X. L. Hu, *Chem. - Eur. J.* **2012**, *18*, 11528-11530; o) B. Hu, D. F. Chen and X. L. Hu, *Chem. - Eur. J.* **2013**, *19*, 6221-6224; p) B. Hu, D. F. Chen and X. L. Hu, *Chem. - Eur. J.* **2014**, *20*, 1677-1682; q) D. F. Chen, R. Scopelliti and X. L. Hu, *Angew. Chem. Int. Ed.* **2011**, *50*, 5671-5673.

[7] For a focus review on [Fe]-hydrogenase models containing iron-acyl ligation see: K.M. Schultz, D.F. Chen, X.L. Hu, Chem.-Asian J. 2013, 8, 1068-1075.

[8] N. Nakatani, Y. Nakao, H. Sato and S. Sakaki, *Chem. Lett.* **2009**, *38*, 958-959.

[9] A. Dey, *J. Am. Chem. Soc.* **2010**, *132*, 13892-13901.

[10] a) M. T. Stiebritz and M. Reiher, *Inorg. Chem.* **2010**, *49*, 5818-5823; b) M. T. Stiebritz, A. R. Finkelmann and M. Reiher, *Eur. J. Inorg. Chem.* **2011**, 1163-1171.

[11] a) J. W. Tye, M. Y. Darensbourg and M. B. Hall, *J. Comput. Chem.* **2006**, *27*, 1454-1462; b) J. W. Tye, M. Y. Darensbourg and M. B. Hall, *Inorg. Chem.* **2008**, *47*, 2380-2388.

[12] a) J. Gubler, A. R. Finkelmann and M. Reiher, *Inorg. Chem.* **2013**, *52*, 14205-14215; b) E. D. Hedegård, S. Knecht, U. Ryde, J. Kongsted and T. Saue, *Phys. Chem. Chem. Phys.* **2014**, *16*, 4853-4863.

[13] M. D. Wodrich and X. L. Hu, *Eur. J. Inorg. Chem.* **2013**, 3993-3999.

[14] a) X. Yang and M. B. Hall, *J. Am. Chem. Soc.* **2008**, *130*, 14036-14037; b) X. Yang and M. B. Hall, *J. Am. Chem. Soc.* **2009**, *131*, 10901-10908; c) A. R. Finkelmann, M. T. Stiebritz and M. Reiher, *Chem. Sci.* **2014**, *5*, 215-221; d) S. Vogt, E. J. Lyon, S. Shima and R. K. Thauer, *J. Biol. Inorg. Chem.* **2008**, *13*, 97-106; e) A. R. Finkelmann, M. T. Stiebritz and M. Reiher, *Chem. Commun.* **2013**, *49*, 8099-8101; f) A. R. Finkelmann, H. M. Senn and M. Reiher, *Chem. Sci.* **2014**, DOI: 10.1039/C1034SC01605J.

[15] a) Y. Zhao and D. G. Truhlar, *Theor. Chem. Acc.* **2008**, *120*, 215-241; b) Y. Zhao and D. G. Truhlar, *Acc. Chem. Res.* **2008**, *41*, 157-167.

[16] A. V. Marenich, C. J. Cramer and D. G. Truhlar, *J. Phys. Chem. B* **2009**, *113*, 4775-4777.

[17] a) S. Miertus, E. Scrocco and J. Tomasi, *Chem. Phys.* **1981**, *55*, 117-129; b) J. Tomasi, B. Mennucci and R. Cammi, *Chem. Rev.* **2005**, *105*, 2999-3093.

[18] M. J. Frisch, G. W. Trucks, H. B. Schlegel, G. E. Scuseria, M. A. Robb, J. R. Cheeseman, G. Scalmani, V. Barone, B. Mennucci, G. A. Petersson, H. Nakatsuji, M. Caricato, X. Li, H. P. Hratchian, A. F. Izmaylov, J. Bloino, G. Zheng, J. L. Sonnenberg, M. Hada, M. Ehara, K. Toyota, R. Fukuda, J. Hasegawa, M. Ishida, T. Nakajima, Y. Honda, O. Kitao, H. Nakai, T. Vreven, J. Montgomery, J. A., J. E. Peralta, F. Ogliaro, M. Bearpark, J. J. Heyd, E. Brothers, K. N. Kudin, V. N. Staroverov, R. Kobayashi, J. Normand, K. Raghavachari, A. Rendell, J. C. Burant, S. S. Iyengar, J. Tomasi, M. Cossi, N. Rega, M. J. Millam, M. Klene, J. E. Knox, J. B. Cross, V. Bakken, C. Adamo, J. Jaramillo, R. Gomperts, R. E. Stratmann, O. Yazyev, A. J. Austin, R. Cammi, C. Pomelli, J. W. Ochterski, R. L. Martin, K. Morokuma, V. G. Zakrzewski, G. A. Voth, P. Salvador, J. J. Dannenberg, S. Dapprich, A. D.

Daniels, O. Farkas, J. B. Foresman, J. V. Ortiz, J. Cioslowski and D. J. Fox in *Gaussian 09, Revision D.01*, *Vol*. Gaussian, Inc., Wallingford, CT, **2009**.
[19] a) A. D. Becke, *J. Chem. Phys.* **1993**, *98*, 5648-5652; b) C. Lee, W. Yang and R. G. Parr, *Phys. Rev. B* **1988**, *37*, 785-789.
[20] a) S. N. Steinmann and C. Corminboeuf, *J. Chem. Theory Comput.* **2011**, 3567-3577; b) S. N. Steinmann and C. Corminboeuf, *J. Chem. Phys.* **2011**, *134*, 044117; c) S. N. Steinmann and C. Corminboeuf, *Chimia* **2011**, *65*, 240-244; d) S. N. Steinmann and C. Corminboeuf, *J. Chem. Theory Comput.* **2010**, *6*, 1990-2001.
[21] a) G. te Velde, F. M. Bickelhaupt, S. J. A. van Gisbergen, C. Fonseca Guerra, E. J. Baerends, J. G. Snijders and T. Ziegler, *J. Comput. Chem.* **2001**, *22*, 931-967; b) C. Fonseca Guerra, J. G. Snijders, G. te Velde and E. J. Baerends, *Theor. Chem. Acc.* **1998**, *99*, 391-403.
[22] ADF2013, SCM, Theoretical Chemistry, Vrije Universiteit, Amsterdam, The Netherlands, http://www.scm.com
[23] a) A. J. Olaya, P. Ge, J. F. Gonthier, P. Pechy, C. Corminboeuf and H. H. Girault, *J. Am. Chem. Soc.* **2011**, *133*, 12115-12123; b) S. Rochat, S. N. Steinmann, C. Corminboeuf and K. Severin, *Chem. Commun.* **2011**, *47*, 10584-10586; c) T. N. Hoheisel, S. Schrettl, R. Marty, T. K. Todorova, C. Corminboeuf, A. Sienkiewicz, R. Scopelliti, W. B. Schweizer and H. Frauenrath, *Nature Chem.* **2013**, *5*, 327-334; d) J. F. Gonthier, S. N. Steinmann, L. Roch, A. Ruggi, N. Luisier, K. Severin and C. Corminboeuf, *Chem. Commun.* **2012**, *48*, 9239-9241; e) M. D. Wodrich, K. O. Zhurov, A. Vorobyev, H. Ben Hamidane, C. Corminboeuf and Y. O. Tsybin, *J. Phys. Chem. B* **2012**, *116*, 10807-10815; f) C. Corminboeuf, *Acc. Chem. Res.* **2014**, DOI:10.1021/ar400303a.
[24] S. N. Steinmann, C. Piemontesi, A. Delachat and C. Corminboeuf, *J. Chem. Theory Comput.* **2012**, *8*, 1629-1640.
[25] P. Ge, T. K. Todorova, I. Hatay Patir, A. J. Olaya, H. Vrubel, M. Mendez, X. L. Hu, C. Corminboeuf and H. H. Girault, *Proc. Natl. Acad. Sci. U.S.A.* **2012**, *109*, 11558-11563.
[26] A. Klamt, *WIREs Comp. Mol. Sci.* **2011**, *1*, 699-709.
[27] S. E. Wheeler and K. N. Houk, *J. Chem. Theory Comput.* **2010**, *6*, 395-404.
[28] a) Y. Mo and S. D. Peyerimhoff, *J. Chem. Phys.* **1998**, *109*, 1687-1697; b) Y. Mo, J. L. Gao and S. D. Peyerimhoff, *J. Chem. Phys.* **2000**, *112*, 5530-5531.
[29] R. Z. Khaliullin, A. T. Bell and M. Head-Gordon, *J. Chem. Phys.* **2008**, *128*, 184112.
[30] Y. Shao, L. Fusti-Molnar, Y. Jung, J. Kussmann, C. Ochsenfeld, S. T. Brown, A. T. B. Gilbert, L. V. Slipchenko, S. V. Levchenko, D. P. O'Neill, R. A. Distasio Jr., R. C. Lochan, T. Wang, G. J. O. Beran, N. A. Besley, J. M. Herbert, C. Y. Lin, T. Van Voorhis, S. H. Chien, A. Sodt, R. P. Steele, V. A. Rassolov, P. E. Maslen, P. P. Korambath, R. D. Adamson, B. Austin, J. Baker, E. F. C. Byrd, H. Dachsel, R. J. Doerksen, A. Dreuw, B. D. Dunietz, A. D. Dutoi, T. R. Furlani, S. R. Gwaltney, A. Heyden, S. Hirata, C.-P. Hsu, G. Kedziora, R. Z. Khalliulin, P. Klunzinger, A. M. Lee, M. S. Lee, W. Liang, I. Lotan, N. Nair, B. Peters, E. I. Proynov, P. A. Pieniazek, Y. M. Rhee, J. Ritchie, E. Rosta, C. D. Sherrill, A. C. Simmonett, J. E. Subotnik, H. L. Woodcock III, W. Zhang, A. T. Bell, A. K. Chakraborty, D. M. Chipman, F. J. Keil, A. Warshel, W. J. Hehre, H. F. Schaefer III, J. Kong, A. I. Krylov, P. M. W. Gill and M. Head-Gordon, *Phys. Chem. Chem. Phys.* **2006**, *8*, 3172-3191.
[31] The negative free energy value results from a combination of single point computations and corrections for solvation. At the optimization level (M06/def2-SVP) the electronic energy gives a TS barrier height of 5.13 kcal/mol (see SI for details).
[32] R. Langer, G. Leitus, Y. Ben-David and D. Milstein, *Angew. Chem., Int. Ed.* **2011**, *50*, 2120-2124.

Graphical Abstract:

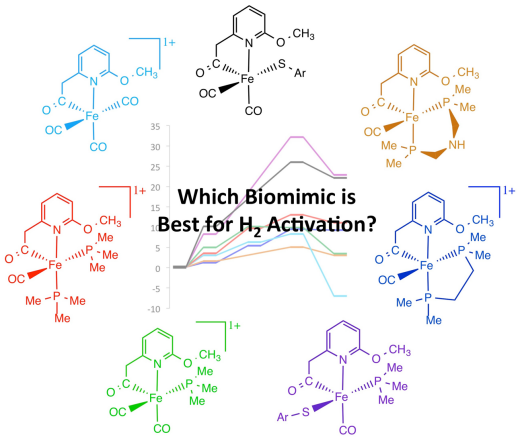

The energetics of seven [Fe]-Hydrogenase biomimics were examined via DFT computations to identify the key factors governing H_2 binding and activating ability. One mimic, with a bidentate diphosphine group containing an internal nitrogen base possesses particularly attractive energetics. Following H_2 binding and heterolytic cleavage, use of a small aldehyde capable of accepting both the proton and hydride, yields a complete catalytic H_2 activation cycle requiring only 14 kcal/mol of energy.

Keywords: Biomimetic Chemistry; Enzyme Models; Hydrogenase; Density Functional Computations; Ligand Effects